

# Anisotropic two- and four-wave mixing in planar LiTaO<sub>3</sub>:Ti:Fe optical waveguides

D. Kip and T. Bartholomäus

Universität Osnabrück, Barbarastrasse 7, 49069 Osnabrück, Germany

P. M. Garcia

Universidade Estadual de Campinas, 13083-970 Campinas, São Paulo, Brazil

E. Krätzig

Universität Osnabrück, Barbarastrasse 7, 49069 Osnabrück, Germany

Received November 12, 1993; revised manuscript received March 10, 1994; accepted March 11, 1994

We report on anisotropic wave mixing in planar iron-doped titanium-indiffused LiTaO<sub>3</sub> waveguides. The diffusion of titanium in Y-cut LiTaO<sub>3</sub> is investigated for different temperatures and diffusion times, yielding the diffusion constant. Material properties of the waveguides such as conductivity and nondiagonal photovoltaic tensor elements are investigated by two-wave mixing of orthogonally polarized modes. Phase conjugation in waveguides by anisotropic four-wave mixing is demonstrated, too, and experimental results are compared with numerical solutions of the corresponding system of coupled-wave equations.

## INTRODUCTION

LiTaO<sub>3</sub> crystals are of increasing interest for the fabrication of integrated optical devices. The higher resistance against optical damage of this substrate material compared with LiNbO<sub>3</sub> permits many applications, e.g., low-voltage electro-optic modulators<sup>1,2</sup> or frequency doublers for blue light.<sup>3</sup> On the other hand, the excellent photorefractive properties,<sup>4</sup> especially of iron- or copper-doped LiTaO<sub>3</sub> waveguides, may also stimulate the development of integrated components such as holographic memory cells or optical amplifiers.<sup>5</sup>

In this paper we report on the fabrication and the investigation of photorefractive LiTaO<sub>3</sub> waveguides. The guides are prepared by titanium indiffusion in homogeneously iron-doped Y-cut substrates, and some of them are additionally doped by iron indiffusion. The photorefractive properties of these waveguides are measured by two-wave mixing of orthogonally polarized waveguide modes.<sup>6</sup> The mechanism of coupling of orthogonally polarized modes is explained by the writing of holographic gratings driven by photovoltaic currents.<sup>7</sup> Anisotropic four-wave mixing permits the generation of phase-conjugate waves in LiTaO<sub>3</sub> waveguides, as already demonstrated for LiNbO<sub>3</sub>.<sup>8</sup> A theoretical description based on coupled-wave equations is also presented.

## THEORY

### Photovoltaic Effect

In LiTaO<sub>3</sub> crystals the redistribution of photoexcited charge carriers is dominated by the photovoltaic effect.<sup>9</sup> Following from a phenomenological theory,<sup>10</sup>

the polarization-dependent photovoltaic current density is given by

$$j_k = \sum_{l,m} (\beta_{klm}^s + i\beta_{klm}^a) E_l^* E_m, \quad (1)$$

where  $\beta_{klm}^{s,a}$  are the real linear ( $s$ , symmetric) and circular ( $a$ , antisymmetric) photovoltaic tensor components and  $E_{l,m}$  are the interacting light fields.

With illumination of the crystal, the photovoltaic current causes the buildup of a periodic space-charge field  $E^{sc}$ , which leads to a perturbation of the dielectric tensor by means of the electro-optic effect:

$$\Delta\epsilon_{ij} = -\epsilon_{is} r_{stk} E_k^{sc} \epsilon_{tj}, \quad (2)$$

where  $r_{stk}$  is the electro-optic tensor component. The perturbation  $\Delta\epsilon$  has unshifted components according to the tensor elements  $\beta_{klm}^s$  and components shifted by  $\pi/2$  according to  $\beta_{klm}^a$ , relative to the isophase surfaces, with a phase difference of the interacting light fields  $E_{l,m}$  of  $2p\pi$ , where  $p = 0, 1, 2, \dots$ . As is well known,<sup>11,12</sup> the shifted grating leads to an energy exchange (beam coupling) between the two interacting beams.

### Anisotropic Wave Mixing

In general, we have the interaction of an extraordinarily (TE-) polarized wave 1 propagating along the  $+x$  axis and two ordinarily (TM-) polarized counterpropagating ( $+x$  and  $-x$ ) waves 2 and 4 in a planar Y-cut LiTaO<sub>3</sub> waveguide (Fig. 1). As was shown in detail in Ref. 6, only orthogonally polarized beams traveling in the same direction can write a grating in this configuration. For counterpropagating beams there is practically no direct

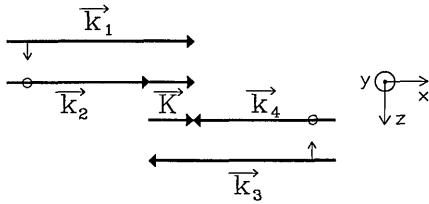


Fig. 1. Interaction scheme of anisotropic wave mixing with  $k_{1,3} = 2\pi n_e^*/\lambda$  as modulus for the TE wave vector,  $k_{2,4} = 2\pi n_o^*/\lambda$  for the TM wave vector, and  $K = 2\pi/\Lambda$  for the grating vector.

interaction or only a small amount; thus reflection gratings (e.g.,  $\mathbf{k}_1 - \mathbf{k}_4$ ) can be neglected here. The waves 1 and 2 write a phase grating with the wave vector  $\mathbf{K} = \mathbf{k}_1 - \mathbf{k}_2$ . Anisotropic diffraction of the wave 4 from this grating generates the extraordinarily (TE-) polarized wave 3, the phase-conjugate replica of the wave 1. The vector of the grating recorded by the waves 3 and 4 is identical to the initial one:

$$\mathbf{k}_4 - \mathbf{k}_3 = \mathbf{k}_1 - \mathbf{k}_2 = \mathbf{K}. \quad (3)$$

The grating period is determined by birefringence:

$$\Lambda = 2\pi/K = \lambda/(n_e^* - n_o^*), \quad (4)$$

where  $n_{e,o}^*$  are the effective refractive indices of the TE- and the TM-polarized modes and  $\lambda$  is the vacuum wavelength of light.

### Space-Charge Field

The total conductivity in the waveguide results from dark conductivity  $\hat{\sigma}_d$  and photoconductivity  $\hat{\sigma}_{ph} = \hat{\sigma}^0 I$  ( $\hat{\sigma}^0$  is the specific photoconductivity):

$$\hat{\sigma}(x, y) = \hat{\sigma}_d + \hat{\sigma}^0 I(x, y), \quad (5)$$

with

$$I(x, y) = \frac{c\epsilon_0}{2} \sum_{i=1}^4 n_i |A_i(x)|^2 |U_i(y)|^2 \exp(\mp \alpha_i x), \quad (6)$$

where the electric field  $\mathbf{E}$  of each wave is separated into an amplitude  $A$  and a normalized electric-field vector (mode)  $\mathbf{U}$ ,  $\mathbf{E}(x, y) = A(x)\mathbf{U}(y)$ . The sign of the exponent ( $\alpha x$ ) depends on the propagation direction and is negative (positive) for the waves 1 and 2 (3 and 4). In our waveguides dark conductivity is small compared with photoconductivity and can be neglected in the following calculation.

In the geometry considered here only the component of the space-charge field in the  $y$  direction leads to a coupling of the interacting waves by means of  $r_{232}$  ( $r_{231} = 0$ ). The space-charge field is proportional to the amplitude of the photovoltaic current divided by conductivity. Thus we can write

$$\begin{aligned} E_{sc,2}(x, y) &= \frac{-1}{\sigma_{22}^0 I(x, y)} (\beta_{232}^s + i\beta_{232}^a) A_{TE}^*(x) \\ &\times A_{TM}(x) U_{sc,2}(y) \cos(Kx). \end{aligned} \quad (7)$$

Using the continuity equation for the total current,  $\text{div}(\mathbf{j}_{ph} + \hat{\sigma}\mathbf{E}_{sc}) = 0$ , and Maxwell's equation  $\text{rot}\mathbf{E}_{sc} = 0$ ,

we obtain a differential equation for the spatial dependence  $U_{sc,2}(y)$  of the space-charge field:

$$\begin{aligned} &\left( \frac{\partial^2}{\partial y^2} - K^2 \right) \frac{U_{sc,2}(y)}{I(x, y)} \\ &= \frac{\partial}{\partial y} \left\{ \frac{-1}{I(x, y)} \left[ \frac{U_{sc,2}(y)}{I(x, y)} \frac{\partial I(x, y)}{\partial y} - \frac{\partial(U_{TE,3} U_{TM,2})}{\partial y} \right] \right\}. \end{aligned} \quad (8)$$

The longitudinal field component of the TM mode ( $U_{TM,1}$ ) is small compared with the transverse component ( $U_{TM,2}$ ) and can be neglected here.

### Coupled-Wave Equations

The coupling equations for two counterpropagating pairs of orthogonally polarized waves can be written in the form<sup>8,13</sup>

$$\frac{dA_1}{dx} = \sqrt{h_2/h_1}/n_e^* (\kappa |A_2|^2 A_1 - \kappa^* A_2 A_4 A_3^*) - \frac{\alpha_e}{2} A_1, \quad (9)$$

$$\frac{dA_2}{dx} = \sqrt{h_1/h_2}/n_o^* (-\kappa |A_1|^2 A_2 + \kappa A_1 A_3 A_4^*) - \frac{\alpha_o}{2} A_2, \quad (10)$$

$$\frac{dA_3}{dx} = \sqrt{h_2/h_1}/n_e^* (-\kappa |A_4|^2 A_3 + \kappa^* A_4 A_2 A_1^*) + \frac{\alpha_e}{2} A_3, \quad (11)$$

$$\frac{dA_4}{dx} = \sqrt{h_1/h_2}/n_o^* (\kappa^* |A_3|^2 A_4 - \kappa A_3 A_1 A_2^*) + \frac{\alpha_o}{2} A_4, \quad (12)$$

with

$$\text{Re}(\kappa) = \frac{\omega n_o^{*2} n_e^{*2}}{2c\sigma_{22}^0} r_{232} \beta_{232}^a \zeta(x), \quad (13)$$

$$\text{Im}(\kappa) = \frac{\omega n_o^{*2} n_e^{*2}}{2c\sigma_{22}^0} r_{232} \beta_{232}^s \zeta(x), \quad (14)$$

$$\zeta(x) = \frac{1}{\sqrt{h_1 h_2}} \int U_{TE,3}(y) \left[ \frac{U_{sc,2}(y)}{I(x, y)} \right] U_{TM,2}(y) dy. \quad (15)$$

Here  $h$  is the effective thickness of the TE and the TM modes, according to the normalization  $\int U_i U_j dy = h_i \delta_{ij}$ ,  $\alpha_{e,o}$  is the extinction coefficient, and  $\omega$  and  $c$  are the frequency and the vacuum speed of light. We have assumed equal modes and extinction coefficients of the waves 1, 3 and 2, 4, respectively. In addition to the space-charge field the complex coupling constant  $\kappa$  is a function of propagation direction.  $\zeta(x)$  describes the overlap of the interacting light fields with the space-charge field, where the spatial distribution  $U_{sc,2}(y)$  follows from Eq. (8).

The first part of the coupled equations (9)–(12) accounts for two-beam coupling between beams 1 and 2 and between beams 3 and 4. The four-wave interaction of the beams 1 and 2 with the grating written by 3 and 4 (and vice versa) is described by the second part. In iron-doped LiTaO<sub>3</sub> waveguides the amplification direction for two-beam coupling is from ordinarily to extraordinarily polarized waves; thus wave 1 and the corresponding phase-conjugate wave 3 are amplified simultaneously because of direct two-beam coupling and four-wave mixing.

### Erasure with Inhomogeneous Illumination

With homogeneous illumination a holographic grating decays exponentially with a time constant  $\tau$  that is inversely proportional to conductivity. If the grating is erased with an excited mode of the waveguide, we have

$$\begin{aligned} \Delta\epsilon_{ij}(x, y, t) &= \Delta\epsilon_{ij}^0(x, y)\exp(-t/\tau) \\ &= \Delta\epsilon_{ij}^0(x, y)\exp\left[-\frac{cn\sigma_0 t}{2\epsilon^{\text{stat}}}\frac{|\mathbf{E}_{\text{erase}}(x, y)|^2}{\exp(-\alpha x)}\right], \end{aligned} \quad (16)$$

where  $\epsilon^{\text{stat}} = \epsilon_{22}^{\text{stat}}$  is the static dielectric constant and  $\mathbf{E}_{\text{erase}}$  is the electric field of the erasing mode.

The decay of the grating is measured by means of the decrease of diffraction efficiency, which is defined as the ratio of diffracted and total light intensity:

$$\eta = \frac{I_{\text{diff}}}{I_{\text{diff}} + I_{\text{trans}}} \quad (17)$$

If we neglect dynamical effects, a modified Kogelnik equation<sup>14</sup> describes the relation of the perturbation  $\Delta\epsilon_{ij}$  of the dielectric tensor and the diffraction efficiency

$$\eta = \sin^2\left(\frac{\pi d}{\lambda} \langle \Delta\epsilon_{23} \rangle_{x,y}\right), \quad (18)$$

with

$$\langle \Delta\epsilon_{23} \rangle_{x,y} = \frac{\int |\mathbf{E}_{\text{read}}(x, y)|^2 \langle \Delta\epsilon_{23} \rangle_x dy}{\int |\mathbf{E}_{\text{read}}(x, y)|^2 dy}, \quad (19)$$

$$\langle \Delta\epsilon_{23} \rangle_x = \frac{1}{d} \int \Delta\epsilon_{23}(x, y) dx. \quad (20)$$

Here  $d$  is the interaction length and  $\mathbf{E}_{\text{read}}$  is the electric field of the mode that reads the hologram.

## EXPERIMENTAL METHODS

### Titanium Indiffusion in LiTaO<sub>3</sub>

Waveguides are prepared by titanium indiffusion (80-nm titanium film, annealed 3–24 h at 1150–1340 °C) in iron-doped (0.01 and 0.02 wt. % Fe<sub>2</sub>O<sub>3</sub>) Y-cut LiTaO<sub>3</sub> substrates. To achieve higher photorefractive sensitivity, in some waveguides an iron film (10 nm, annealed 2 h at 1300 °C) is additionally indiffused after titanium indiffusion.

The effective refractive indices of the TE and the TM modes of the waveguides are measured by the prism coupling method (dark-line spectroscopy). From the effective refractive indices the profiles of ordinary and extraordinary refractive indices are reconstructed by an inverse WKB method.<sup>15</sup>

The penetration depth of titanium in the LiTaO<sub>3</sub> substrates is large compared with the thickness of the vacuum-deposited titanium layer. Thus we expect that the concentration profile of titanium can be described by a Gaussian function<sup>16</sup> (diffusion from a finite source):

$$c_{\text{Ti}}(y) = c_{\text{Ti}}^0 \exp(-y^2/2\rho^2), \quad (21)$$

$$\rho = \sqrt{2Dt}, \quad (22)$$

$$D = D_0 \exp(-E/k_B T). \quad (23)$$

The penetration depth  $\rho$  depends on the temperature-

dependent diffusion constant  $D$  and the diffusion time  $t$ .  $D_0$  is the diffusion coefficient;  $E$ , the activation energy;  $k_B$ , the Boltzmann constant; and  $T$ , the temperature.

### Poling and Reduction Treatment

After titanium indiffusion at high temperatures far above the Curie temperature of 620 °C, the LiTaO<sub>3</sub> waveguides must be repoled. Therefore we apply an electric field of approximately 20 V cm<sup>-1</sup> in the  $z$  direction and anneal the waveguides for approximately 15 min at 650 °C. Poling is controlled by measurement of the pyroelectric current  $I = A(dP_s/dT)_T(dT/dt)$ , where  $A$  is the area of the gold electrodes and  $(dP_s/dT)_T$  is the pyroelectric coefficient. With a heating rate of  $(dT/dt) = 0.5 \text{ K s}^{-1}$ , we obtain a value of  $(dP_s/dT)_T = (2.1 \pm 0.1) \times 10^{-8} \text{ C cm}^{-2} \text{ K}^{-1}$ , which is in fairly good agreement with other results [e.g.,  $(1.9 \pm 0.1) \times 10^{-8} \text{ C cm}^{-2} \text{ K}^{-1}$  in Ref. 17].

To increase the Fe<sup>2+</sup> concentration and thereby the holographic sensitivity, the waveguides are reduced in an oxygen-deficient atmosphere. The samples are wrapped in platinum foil together with Li<sub>2</sub>CO<sub>3</sub> (Ref. 18) and are annealed for several hours at temperatures in the range of 410–550 °C.

### Setup for Holographic Measurements

The experimental setup is shown in Fig. 2. We use light of the green line (514.5 nm) of an Ar<sup>+</sup>-ion laser. The light is split into three different beams and is coupled into polarization-conserving monomode fibers. Care must be taken to obtain equal optical-path lengths. Rutile prisms are used to couple radiation into and out of the waveguide. The input coupling efficiency is measured to be approximately 70%. We assume an output coupling efficiency of 100% because in this case the input losses that are due to the Gaussian shape of the beam do not occur. The beam size of the three beams is adjusted to be 0.4 mm, and the interaction length is 5.0 mm.

### Determination of Conductivity

Dark conductivity is measured by the relaxation of a phase grating without illumination. Gratings are written with a combination of a TE and a TM mode, and after saturation the diffraction efficiency is measured with a low-power reading beam as a function of time. Photoconductivity is determined by the erasure of a written phase grating with either a guided TE mode or a

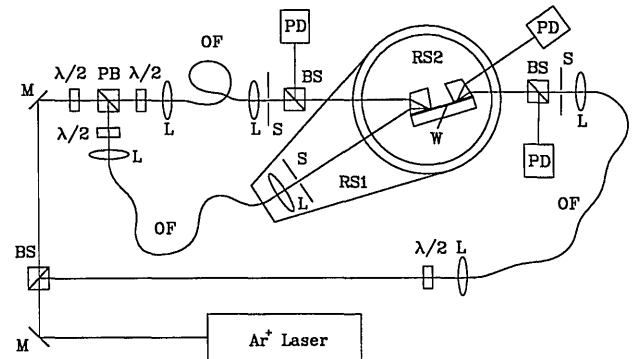


Fig. 2. Experimental arrangement for anisotropic wave mixing in a LiTaO<sub>3</sub> waveguide. M's, mirrors; BS's, beam splitters; PB, polarizing beam splitter;  $\lambda/2$ 's, half-wave plates; L's, microscope lenses; OF's, optical fibers; S's, shutters; RS1, RS2, rotary stages; PD's, photodetectors; W, waveguide.

**Table 1. Parameters of Titanium Indiffusion and Measured Penetration Depths  $\rho_{o,e}$  of the Waveguides LT10–LT17, Obtained from the Reconstructed Ordinary ( $\rho_o$ ) and Extraordinary ( $\rho_e$ ) Refractive-Index Profiles<sup>a</sup>**

Sample	$t$ (h) <sup>b</sup>	$T$ (°C) <sup>c</sup>	$\rho_o$ ( $\mu\text{m}$ ) <sup>d</sup>	$\rho_e$ ( $\mu\text{m}$ ) <sup>e</sup>
LT10	3	1300	2.94	3.00
LT11	6	1300	4.53	4.49
LT12	12	1300	6.33	6.39
LT13	24	1150	2.69	2.71
LT14	24	1200	4.00	4.00
LT15	24	1250	6.33	6.27
LT17	24	1300	8.47	8.11

<sup>a</sup> The thickness of the vacuum-deposited titanium layer is 80 nm for the waveguides LT10–LT15 and 200 nm for the waveguide LT17. All the waveguides are homogeneously iron doped (0.01 wt. % Fe<sub>2</sub>O<sub>3</sub>).

<sup>b</sup> Annealing time.

<sup>c</sup> Temperature.

<sup>d</sup> For TM-polarized-mode refractive index  $n_o$ .

<sup>e</sup> For TE-polarized-mode refractive index  $n_e$ .

guided TM mode. Then Eqs. (16) and (18)–(20) are fitted to the measured relaxation of the grating, yielding  $\sigma_{22}^0 = \sigma_{22}/I$ .

### Measurement of Photovoltaic Tensor Elements

For measurement of the photovoltaic tensor elements  $\beta_{232}^s$  and  $\beta_{232}^a$ , beam coupling and anisotropic diffraction of the TE and the TM modes are evaluated. The energy exchange between the two orthogonally polarized modes results from the real part of the coupling constant [Eq. (13)] proportional to  $\beta_{232}^a$ , whereas the diffraction efficiency of the grating is determined by the modulus of the coupling constant,  $|\kappa| \propto |i\beta_{232}^s + \beta_{232}^a|$ . Thus fitting Eqs. (9) and (10) with  $A_{3,4} = 0$  to the measured values of the energy exchange and the diffraction efficiency yields  $|\beta_{232}^s|$  and  $\beta_{232}^a$ .

## RESULTS AND DISCUSSION

### Titanium Indiffusion in LiTaO<sub>3</sub>

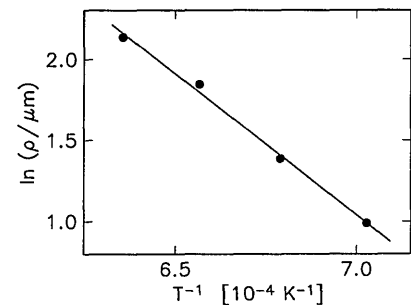
In Table 1 the parameters of titanium indiffusion and measured penetration depths  $\rho_{o,e}$  of the LiTaO<sub>3</sub> waveguides LT10–LT17 are listed. We obtain the penetration depth by fitting Eq. (21) to the reconstructed refractive-index profiles for ordinary ( $\rho_o$ ) and extraordinary ( $\rho_e$ ) polarization, respectively. All the refractive-index profiles can be well described by Gaussian functions. The linear dependence of refractive-index changes  $\Delta n_e$  and  $\Delta n_o$  on titanium concentration in LiTaO<sub>3</sub> is verified by microprobe investigations, as described in Ref. 16.

By fitting Eqs. (22) and (23) to the measured penetration depths given in Table 1 we obtain the values of the diffusion coefficient and the activation energy for the diffusion of titanium in LiTaO<sub>3</sub>. The results are shown in Fig. 3, and from the linear approximations we obtain  $D_0 = 5.5 \times 10^{-3} \text{ cm}^2 \text{ s}^{-1}$  and  $E = 3.0 \text{ eV}$ . For a temperature of  $T = 1300 \text{ }^\circ\text{C}$  this yields a diffusion constant of  $D_{1300 \text{ }^\circ\text{C}} = 1.3 \times 10^{-12} \text{ cm}^2 \text{ s}^{-1}$ , which is comparable with  $D_{1300 \text{ }^\circ\text{C}} = 4.8 \times 10^{-13} \text{ cm}^2 \text{ s}^{-1}$  in Ref. 19. The difference can perhaps be explained by the different Li/Ta ratios of the substrate materials. This ratio exerts a strong influence on the diffusion of titanium in LiTaO<sub>3</sub>.<sup>20</sup>

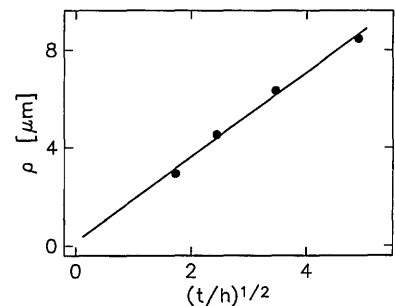
### Conductivity

The relaxation of a phase grating in the dark that has been written up to saturation can be seen in Fig. 4 for the waveguide LT10. The diffraction efficiency is measured by short reading (0.1 s with a TM mode) of the hologram in time intervals of 1 h. The relaxation is monoexponential with a time constant  $\tau = 6.4 \text{ h}$  (solid curve), where the influence of the reading beam has been taken into account. With  $\epsilon_{22}^{\text{stat}} = 51.0$  we obtain a dark conductivity of  $\sigma_d = 2.0 \times 10^{-14} \text{ V A}^{-1} \text{ m}^{-1}$ . With usual intensities inside the waveguide of several kilowatts per square meter the influence of dark conductivity compared with photoconductivity is small and is neglected in the discussion below.

Figure 5 shows the specific conductivity  $\sigma_{22}^0$  as a func-



(a)



(b)

Fig. 3. (a) Logarithm of penetration depth  $\rho = (\rho_e + \rho_o)/2$  as a function of inverse temperature  $T^{-1}$ . Depth  $\rho$  as a function of the square root of the diffusion time  $t$ . The solid lines are linear approximations yielding the diffusion coefficient  $D_0$  and the activation energy  $E$  from Eqs. (22) and (23), respectively.

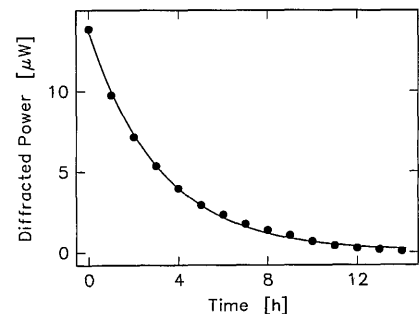


Fig. 4. Relaxation of a phase grating for the waveguide LT10. The diffraction efficiency is measured by short reading (0.1 s with a TM mode) of the hologram in time intervals of 1 h. The solid curve shows a monoexponential approximation of the decay with a time constant  $\tau = 6.4 \text{ h}$ .

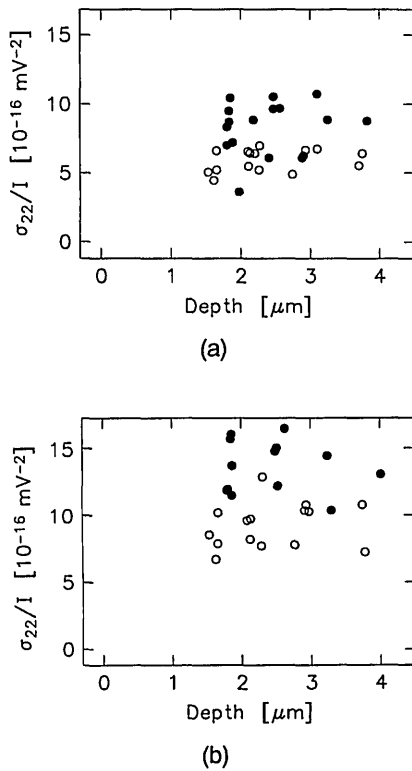


Fig. 5. Specific photoconductivity as a function of depth for the waveguide LT11. Evaluated is the relaxation of phase gratings that are due to illumination with either TE (extraordinarily polarized, open circles) or TM (ordinarily polarized, filled circles) modes. The waveguide was investigated in two different oxidation states. (a) Reduced for 10 h at 510 °C, (b) additionally reduced for 10 h at 550 °C.

tion of depth for the waveguide LT11. We evaluate the relaxation of phase gratings that have been written by combinations of TE and TM modes ( $\text{TE}_i$ ,  $\text{TM}_j$ ,  $i, j = 0 \dots 3$ ) with different effective propagation depths inside the waveguide. The gratings are erased with either (extraordinarily polarized) TE or (ordinarily polarized) TM modes. The waveguide was investigated in two different oxidation states. In a first step it was reduced for 10 h at 510 °C [Fig. 5(a)], and in a second step it was additionally reduced for 10 h at 550 °C [Fig. 5(b)].

The specific photoconductivity for ordinarily polarized light exceeds the values for extraordinary polarization, and no specific dependence on propagation depth is observed. Averaging over all data for each polarization gives a ratio of 1.5 of the specific photoconductivities for ordinarily and extraordinarily polarized light independent of the oxidation state of the waveguide. This is in qualitative agreement with the higher absorption coefficient for ordinarily polarized light in  $\text{LiTaO}_3$ . After the second reduction treatment photoconductivity increases for both polarizations by a factor of 1.6.

#### Photovoltaic Tensor Elements

The measured photovoltaic constants  $|\beta_{232}^s|$  and  $\beta_{232}^a$  of the waveguide LT11 are shown in Fig. 6 for two different oxidation states (see Fig. 5 for details). The photovoltaic tensor elements depend on the  $\text{Fe}^{2+}$  concentration, which is adjusted by annealing. Here the total iron content of our samples (0.01 or 0.02 wt. %  $\text{Fe}_2\text{O}_3$ ) is of minor importance.

The sign of  $\beta_{232}^a$  is positive, resulting in an energy exchange from ordinarily to extraordinarily polarized light. Corresponding data for  $\text{LiTaO}_3$  bulk crystals are not available, but for copper-doped  $\text{LiTaO}_3$  a coupling direction from extraordinarily to ordinarily polarized light was reported.<sup>21</sup> The sign of  $\beta_{232}^s$  cannot be determined from our measurements.

Both the symmetric and the antisymmetric components of the photovoltaic constants increase with increasing propagation depth. One possible reason may be the influence of the high titanium concentration at the surface. This is supported by measurements with heavily doped bulk crystals (0.038 wt. % iron), in which the photovoltaic constants  $\beta_{232}^s$  are more than 1 order of magnitude higher.<sup>22</sup>

On the average the values of  $|\beta_{232}^s|$  are at least a factor of 2 larger than those of  $\beta_{232}^a$ . The dominating non-shifted grating that is due to  $|\beta_{232}^s|$  results in fluctuations of the energy exchange during two-beam coupling caused by phase perturbations of the experimental setup. This is the main reason for the scattering of the measured photovoltaic constants as a function of propagation depth. After the second reduction treatment of the waveguide LT11 the photovoltaic constants are increased (because of higher  $\text{Fe}^{2+}$  concentration) by a factor of 1.5.

#### Phase-Conjugate Waves

For the generation of phase-conjugate waves, we increase the iron content of a  $\text{LiTaO}_3$  waveguide by indiffusion of a thin iron layer (10 nm of iron indiffused for 2 h at 1300 °C,

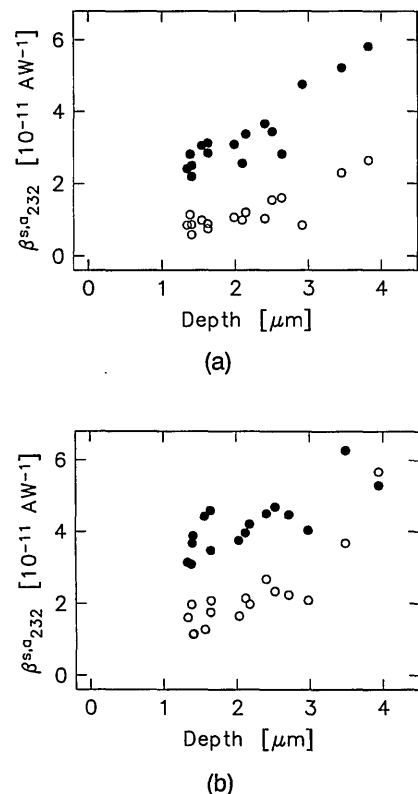


Fig. 6. Photovoltaic constants  $|\beta_{232}^s|$  (filled circles) and  $\beta_{232}^a$  (open circles) as a function of depth for the waveguide LT11. The values are obtained by measurement of energy exchange and diffraction efficiency of anisotropic two-wave mixing for two different oxidation states of the  $\text{LiTaO}_3$  waveguide. (a) Reduced for 10 h at 510 °C, (b) additionally reduced for 10 h at 550 °C.

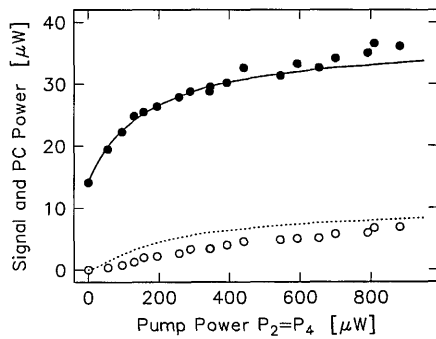


Fig. 7. Dependence of signal wave power [filled circles, experimental; solid curve, theoretical, according to Eqs. (9)–(12)] and phase-conjugate (PC) wave power (open circles, experimental; dotted curve, theoretical) on the power of one input pump wave. The input power of the signal wave is  $80 \mu\text{W}$ . All the values are the powers in the waveguide.

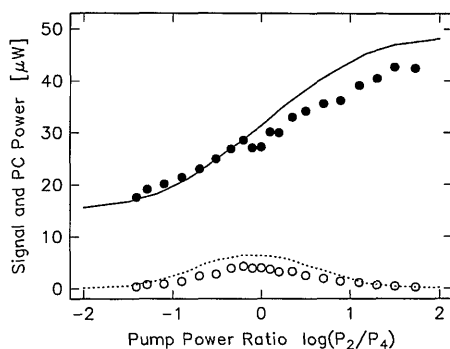


Fig. 8. Dependence of signal wave power [filled circles, experimental; solid curve, theoretical, according to Eqs. (9)–(12)] and phase-conjugate (PC) wave power (open circles, experimental; dotted curve, theoretical) on the ratio of pump wave power. The total pump power is constant,  $P_2 + P_4 = 850 \mu\text{W}$ , and the input power of the signal wave is  $80 \mu\text{W}$ . All the values are the powers in the waveguide.

with other parameters as for LT10). The higher concentration of  $\text{Fe}^{3+}$  in the waveguide causes an increase of the amplitude of the space-charge field,  $E_{sc} \propto \beta_{232}/\sigma_{ph} \propto c_{\text{Fe}^{3+}}$ . Thus the additional incorporation of iron in the sample leads to a stronger coupling of the interacting light waves.

Figure 7 illustrates the dependence of the amplified signal wave and the generated phase-conjugate wave on pump power. The signal and the corresponding phase-conjugate wave are  $\text{TE}_0$  modes, and the two counter-propagating pump waves are  $\text{TM}_0$  modes. These modes have an effective thickness of  $h_{\text{TE}} = 2.05 \mu\text{m}$  and  $h_{\text{TM}} = 2.01 \mu\text{m}$ , respectively. The symbols denote measured values, and the curves represent solutions of the corresponding coupled-wave equations (9)–(12). Here we use the parameters  $\sigma_{22}^0 = 6.3 \times 10^{-17} \text{ m V}^{-2}$ ,  $\beta_{232}^s = 8.5 \times 10^{-12} \text{ A W}^{-1}$ , and  $\beta_{232}^a = 6.5 \times 10^{-12} \text{ A W}^{-1}$  obtained by measurement of two-beam coupling and diffraction efficiency. The input power of the signal wave is  $80 \mu\text{W}$ , and the extinction coefficients are  $\alpha_{\text{TE}} = 346 \text{ m}^{-1}$  and  $\alpha_{\text{TM}} = 320 \text{ m}^{-1}$ .

After a fast increase for low pump power both signal and phase-conjugate wave power increase only slowly. This result is due to the simultaneous increase of photoconductivity, which reduces the amplitude of the space-charge field. For comparison, in  $\text{LiNbO}_3$  waveguides in

which dark conductivity dominates, we observe a steep increase of signal and phase-conjugate wave power for higher pump power.<sup>8</sup> For the highest pump power we have an efficiency of phase conjugation of 9%. The agreement of the theoretical curves with the experimental data is fairly good. Furthermore, we do not observe any amplified stray light resulting from holographic scattering, as in former experiments with  $\text{LiNbO}_3$  waveguides.

The dependence of signal wave power and phase-conjugate wave power on the ratio of pump wave power  $P_2/P_4$  is presented in Fig. 8. In the experiment the total pump wave power  $P_2 + P_4 = 850 \mu\text{W}$  is constant. At the right end,  $P_2 \gg P_4$ , we practically have the case of two-beam coupling, and amplification of the signal wave is strongest. The maximum of phase-conjugate wave power is obtained for nearly equal powers of the two pump beams. The slight shift from equal pump powers results from the asymmetry in the experiment introduced by the high absorption in the waveguide.

The measured values are in good agreement with the calculation, which confirms the existence of a dominating transmission grating in the sample. In this experiment we also observe a weak coupling of the signal wave with the counterpropagating pump wave by means of a reflection grating, but the effect on the amplification of signal and phase-conjugate waves is rather small.

## CONCLUSIONS

In summary, we have shown that photorefractive iron-doped  $\text{LiTaO}_3$  waveguides permit efficient wave mixing of orthogonally polarized light waves. The diffusion of titanium in Y-cut  $\text{LiTaO}_3$  substrates has been investigated, and conductivity and nondiagonal elements of the photovoltaic tensor of the waveguides are measured as a function of propagation depth in the waveguiding layer.

We have observed efficient anisotropic four-wave mixing in  $\text{LiTaO}_3$  waveguides with reflectivities of the phase-conjugate signal to as much as 9%. Both experimental values and the calculation show a saturation behavior of the power of the phase-conjugate wave for high pump power, which is due to the increasing conductivity in the waveguide.

## ACKNOWLEDGMENTS

The financial support of the Deutsche Forschungsgemeinschaft (SFB 225, D9) and the Volkswagen-Stiftung is gratefully acknowledged.

## REFERENCES

1. A. Donaldson, "Candidate materials and technologies for integrated optics: fast and efficient electro-optic modulation," *J. Phys. D* **24**, 785 (1991).
2. T. Findakly, P. Suchoski, and F. Leonberger, "High quality  $\text{LiTaO}_3$  integrated-optical waveguides and devices fabricated by the annealed-proton-exchange technique," *Opt. Lett.* **13**, 797 (1988).
3. K. Mizuuchi and K. Yamamoto, "Characteristics of periodically domain-inverted  $\text{LiTaO}_3$ ," *J. Appl. Phys.* **72**, 5061 (1992).
4. E. Krätzig and R. Orłowski, " $\text{LiTaO}_3$  as holographic storage material," *Appl. Phys.* **15**, 133 (1978).
5. V. E. Wood, P. J. Cressman, R. L. Holman, and C. M. Verber, "Photorefractive effects in waveguides," in *Photorefractive*

- Materials and Their Applications*, P. Günter and J.-P. Huignard, eds., Vol. 62 of Topics in Applied Physics (Springer-Verlag, Berlin, 1989), pp. 45–100.
6. D. Kip, R. Fink, T. Bartholomäus, and E. Krätzig, "Coupling of orthogonally polarized waves in  $\text{LiNbO}_3$  optical waveguides," *Opt. Commun.* **95**, 33 (1993).
  7. S. G. Odoulov, "Vectorial interactions in photovoltaic media," *Ferroelectrics* **91**, 213 (1989).
  8. D. Kip and E. Krätzig, "Anisotropic four-wave mixing in planar  $\text{LiNbO}_3$  optical waveguides," *Opt. Lett.* **17**, 1563 (1992).
  9. A. M. Glass, D. von der Linde, and T. J. Negran, "High voltage bulk photovoltaic effect and the photorefractive process in  $\text{LiNbO}_3$ ," *Appl. Phys. Lett.* **25**, 233 (1974).
  10. V. I. Belinicher and B. Sturman, "The photogalvanic effect in media lacking a center of symmetry," *Sov. Phys. Usp.* **23**, 199 (1980).
  11. S. G. Odoulov and M. S. Soskin, "Amplification, oscillation, and light-induced scattering in photorefractive crystals," in *Photorefractive Materials and Their Applications*, P. Günter and J.-P. Huignard, eds., Vol. 62 of Topics in Applied Physics (Springer-Verlag, Berlin, 1989), pp. 5–43.
  12. D. L. Staebler and J. J. Amodei, "Coupled-wave analysis of holographic storage in  $\text{LiNbO}_3$ ," *J. Appl. Phys.* **43**, 1042 (1972).
  13. A. Novikov, S. G. Odoulov, O. Oleinik, and B. Sturman, "Beam-coupling, four-wave mixing and optical oscillation due to spatially-oscillating photovoltaic currents in lithium niobate crystals," *Ferroelectrics* **75**, 295 (1987).
  14. H. Kogelnik, "Coupled wave theory for thick hologram gratings," *Bell Syst. Tech. J.* **48**, 2909 (1969).
  15. P. Hertel and H. P. Menzler, "Improved inverse WKB procedure to reconstruct index profiles of dielectric planar waveguides," *Appl. Phys. B* **44**, 75 (1987).
  16. D. Kip, B. Gather, H. Bendig, and E. Krätzig, "Concentration and refractive index profiles of titanium- and iron-diffused planar  $\text{LiNbO}_3$  waveguides," *Phys. Status Solidi A* **139**, 241 (1993).
  17. A. M. Glass, "Dielectric, thermal, and pyroelectric properties of ferroelectric  $\text{LiTaO}_3$ ," *Phys. Rev.* **172**, 564 (1968).
  18. W. Phillips and D. L. Staebler, "Control of the  $\text{Fe}^{2+}$  concentration in iron-doped lithium niobate," *J. Electron. Mater.* **3**, 601 (1974).
  19. V. V. Atuchin, K. K. Ziling, and D. P. Shipilova, "Investigation of optical waveguides fabricated by titanium diffusion in  $\text{LiTaO}_3$ ," *Sov. J. Quantum Electron.* **14**, 671 (1984).
  20. V. V. Atuchin and K. K. Ziling, "Effect of the composition of crystals on the parameters of  $\text{LiNbO}_3:\text{Ti}$  and  $\text{LiTaO}_3:\text{Ti}$  optical waveguides," *Sov. Phys. Tech. Phys.* **35**, 488 (1990).
  21. S. G. Odoulov, K. Belabaev, and I. Kiseleva, "Degenerate stimulated parametric scattering in  $\text{LiTaO}_3:\text{Cu}$ ," *Opt. Lett.* **10**, 31 (1985).
  22. S. I. Karabekian and S. G. Odoulov, "Bulk photovoltaic effect in  $\text{LiTaO}_3:\text{Fe}$  crystals," *Phys. Status Solidi B* **169**, 529 (1992).